










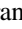



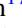






Implications for the Formation of (155140) 2005 UD from a New Convex Shape Model

Jay K. Kueny^{1,2,3,19} , Colin Orion Chandler^{4,5,19} , Maxime Devogèle⁶ , Nicholas Moskovitz¹ , Petr Pravec⁷ ,
Hana Kučáková^{7,8,9} , Kamil Hornoch⁷ , Peter Kušnirák⁷ , Mikael Granvik^{10,11} , Christina Konstantopoulou^{12,13} ,
Nicholas E. Janssen^{13,14} , Shane Moran^{13,15} , Lauri Siltala¹⁰ , Grigori Fedorets^{10,16} , Marin Ferrais^{17,18} ,
Emmanuel Jehin¹⁷ , Theodore Karetá¹ , and Josef Hanuš⁸ 

¹Lowell Observatory, 1400 W. Mars Hill Rd., Flagstaff, AZ 86001, USA

²Steward Observatory, University of Arizona, Tucson, 933 N. Cherry Avenue, Tucson, AZ 85721, USA

³Wyant College of Optical Sciences, University of Arizona, 1630 E. University Boulevard, Tucson, AZ 85721, USA

⁴Department of Astronomy and Planetary Science, Northern Arizona University, PO Box 6010, Flagstaff, AZ 86011, USA

⁵Dept. of Astronomy & the DiRAC Institute, University of Washington, 3910 15th Avenue NE, Seattle, WA 98195, USA

⁶Arecibo Observatory, University of Central Florida, HC-3 Box 53995, Arecibo, PR 00612, USA

⁷Astronomical Institute, Academy of Sciences of the Czech Republic, Fričova 1, CZ-25165 Ondřejov, Czech Republic

⁸Institute of Astronomy, Faculty of Mathematics and Physics, Charles University, V Holešovickách 2, 18000 Prague, Czech Republic

⁹Research Centre for Theoretical Physics and Astrophysics, Institute of Physics, Silesian University in Opava, Bezučovo nám. 13, 74601 Opava, Czech Republic

¹⁰Department of Physics, P.O. Box 64, FI-00014 University of Helsinki, Finland

¹¹Asteroid Engineering Laboratory, Luleå University of Technology, Box 848, SE-98128 Kiruna, Sweden

¹²Department of Astronomy, University of Geneva, Chemin Pegasi 51, 1290 Versoix, Switzerland

¹³Nordic Optical Telescope, Apartado 474, E-38700 Santa Cruz de La Palma, Spain

¹⁴Institute of Astronomy, Celestijnenlaan 200D bus 2401, B-3001 Leuven, Belgium

¹⁵Department of Physics and Astronomy, University of Turku, Vesilinnantie 5, FI-20500, Finland

¹⁶Astrophysics Research Centre, School of Mathematics and Physics, Queen's University Belfast, Belfast BT7 1NN, UK

¹⁷Space sciences, Technologies & Astrophysics Research (STAR) Institute University of Liège Allée du 6 Août 19, B-4000 Liège, Belgium

¹⁸Aix Marseille Univ, CNRS, LAM, Laboratoire d'Astrophysique de Marseille, Marseille, France

Received 2022 September 1; revised 2023 February 27; accepted 2023 March 1; published 2023 March 31

Abstract

(155140) 2005 UD has a similar orbit to (3200) Phaethon, an active asteroid in a highly eccentric orbit thought to be the source of the Geminid meteor shower. Evidence points to a genetic relationship between these two objects, but we have yet to fully understand how 2005 UD and Phaethon could have separated into this associated pair. Presented herein are new observations of 2005 UD from five observatories that were carried out during the 2018, 2019, and 2021 apparitions. We implemented light curve inversion using our new data, as well as dense and sparse archival data from epochs in 2005–2021, to better constrain the rotational period and derive a convex shape model of 2005 UD. We discuss two equally well-fitting pole solutions ($\lambda = 116^\circ.6$, $\beta = -53^\circ.6$) and ($\lambda = 300^\circ.3$, $\beta = -55^\circ.4$), the former largely in agreement with previous thermophysical analyses and the latter interesting due to its proximity to Phaethon's pole orientation. We also present a refined sidereal period of $P_{\text{sid}} = 5.234246 \pm 0.000097$ hr. A search for surface color heterogeneity showed no significant rotational variation. An activity search using the deepest stacked image available of 2005 UD near aphelion did not reveal a coma or tail but allowed modeling of an upper limit of $0.04\text{--}0.37$ kg s^{-1} for dust production. We then leveraged our spin solutions to help limit the range of formation scenarios and the link to Phaethon in the context of nongravitational forces and timescales associated with the physical evolution of the system.

Unified Astronomy Thesaurus concepts: [Near-Earth objects \(1092\)](#); [CCD photometry \(208\)](#); [Light curves \(918\)](#)

Supporting material: data behind figure

1. Introduction

Near-Earth asteroid (NEA) 2005 UD is a kilometer-class object and is a potential flyby target of JAXA's DESTINY⁺ mission,²⁰ scheduled to launch within the next decade. It was discovered in 2005 by the Catalina Sky Survey (Christensen et al. 2005) and was revealed to have an orbit similar to (3200) Phaethon and the Geminid meteor stream. A subsequent observational campaign revealed surface color variations as a function of rotational phase (Kinoshita et al. 2007). Previous

studies on the visible reflectance spectrum suggest that 2005 UD is a B-type asteroid (Jewitt & Hsieh 2006; Devogèle et al. 2020), though recent findings regarding the near-infrared spectrum by Karetá et al. (2021) and a phase curve analysis by Huang et al. (2021) contest this. It is in the Apollo dynamical class with a semimajor axis of 1.275 au, an eccentricity of 0.87, and an orbital inclination of $28^\circ.7$ (see Appendix A for a comprehensive reference table). Light curve inversion by Huang et al. (2021) using the Lommel–Seeliger ellipsoid method yielded a 2005 UD spin pole solution of $(285^\circ.8_{-5.3}^{+1.1}, -25^\circ.8_{-12.5}^{+5.3})$, which is comparable to that of Phaethon (Hanusš et al. 2018, Kim et al. 2018). A common origin with Phaethon continues to be extensively investigated (see, e.g., Devogèle et al. 2020; Karetá et al. 2021; MacLennan et al. 2021).

Asteroid (3200) Phaethon is a B-type NEA (Licandro et al. 2007) and exhibits short bursts of activity at perihelion

¹⁹ National Science Foundation Graduate Research Fellow.

²⁰ <https://destiny.isas.jaxa.jp/science/>



suspected to be caused by thermal fracturing (Jewitt & Li 2010; Jewitt 2012). It has a semimajor axis of 1.271 au, an eccentricity of 0.89, and an orbital inclination of 22.3° . Phaethon is thought to be the parent body of the annual Geminid meteor shower (Whipple 1983), although predicted upper limits to its current dust production rates cannot explain the inferred mass contained within the Geminid meteor stream (Ryabova 2017; Kasuga & Masiero 2022).

Based on dynamical arguments (Ohtsuka et al. 2006; Hanaš et al. 2016; MacLennan et al. 2021) 2005 UD and Phaethon could have split from a larger precursor body at some point in the past, which may explain the aforementioned mass discrepancy with the Geminids. A recent study of the Daytime Sextantids meteor shower (part of the Phaethon–Geminid stream complex) by Kipreos et al. (2022) reinforces this by suggesting that this meteor stream, 2005 UD, and Phaethon were created from a mutual breakup event. This common origin theory is further supported since B-type near-Earth objects are uncommon (Jewitt & Hsieh 2006), and the previously mentioned color variability discovered on 2005 UD begs interesting implications for fresh surface material perhaps due to recent detachment. Analyses of 2005 UD and Phaethon’s polarimetric phase curve by Devogèle et al. (2020) and Ishiguro et al. (2022) reveal similarities over broad phase-angle coverage, again hinting at a genetic relation between the pair. However, counterpoints to the common origin narrative were made by Kareta et al. (2021), who found that these two objects have distinctly different spectral features in the near-infrared, and by Ryabova et al. (2019) based on dynamical tests probing the past 5000 yr.

In this work, we present further constraints on 2005 UD’s rotation period, pole orientation, and shape model through light curve inversion using data from new 2018, 2019, and 2021 observations and archival data. We introduce the observations, data reduction, and shape modeling procedures in the next section. In Section 3, we discuss the refined sidereal period and spin axis orientation for 2005 UD, as well as comment on the current state of a convex shape model. In Section 4 we infer the most likely pole solution for 2005 UD and present our search for surface color heterogeneity and activity. Section 5 leverages our spin solutions to inform possible formation scenarios for 2005 UD. We then conclude with Section 6 and encourage avenues for future work.

2. Data Collection and Processing

We define “light curve” as the time series of disk-integrated brightness of the asteroid collected at a single site in a single filter. We adopt the terms “dense” and “sparse” to describe the two modalities of light curves used in our shape modeling process. Dense light curves feature photometric data points spaced closely in time relative to the rotational period of the object, while sparse light curves typically contain interspersed points and light curve subsections fewer than about seven points per night, spanning greater than 30 days, and are usually the product of nightly astronomical surveys. In total, we used 79 dense and 5 sparse light curves of 2005 UD from apparitions in 2005–2021 for our investigation. Of the set of dense light curves, we included 36 from Devogèle et al. (2020), 10 from Warner & Stephens (2019), 4 from Jewitt & Hsieh (2006), 4 from Kinoshita et al. (2007), and the remaining from our own observations conducted in 2018, 2019, and 2021.

2.1. Observations and Photometry

We present photometric observations of 2005 UD obtained using the following telescopes: the Ondřejov Observatory 0.65 m telescope, the Danish 1.54 m Telescope, North 0.6 m TRANSiting Planets and Planetesimals Small Telescopes (TRAPPIST-N), the 4.3 m Lowell Discovery Telescope (LDT), and the 2.6 m Nordic Optical Telescope (NOT). Our analysis also includes sparse data sets from various surveys (discussed below). Tables B1, B2, and B3 provide details about the observing circumstances.

We used the 4.3 m Lowell Discovery Telescope (LDT), located in Happy Jack, Arizona, USA) on the nights of UT 2019 October 19, 2019 November 18, and 2021 November 3. Images were captured using a broadband VR filter (approximately encompassing the Johnson–Cousins *V* and *R* bands) and the Large Monolithic Imager, which features 6144×6160 pixels and a square $12.5'$ field of view. This instrument samples at a pixel scale of $0''.12 \text{ pixel}^{-1}$ but was used in 3×3 binning mode. Exposure times ranged from 60 to 120 s for the first night, from 14 to 20 s for the second, and from 30 to 35 s for the last. Seeing conditions were very stable for the first and last night and stable at the 25% level for the second night. We recorded median FWHM values of on-chip point sources of about $2''.7$, $1''.5$, and $2''.3$ for the first, middle, and last night, respectively.

The 2.6 m NOT is located at the Spanish Observatorio del Roque de los Muchachos, La Palma, Canarias, Spain. For these data the NOT imaged with the Alhambra Faint Object Spectrograph and Camera (ALFOSC), which equips a nearly square 2048×2064 pixel detector sampled at $0''.21 \text{ pixel}^{-1}$. Observations were carried out on the nights of UT 4 November 2019 and 18 November 2019 in the Sloan Digital Sky Survey (SDSS) *r* filter and with a SDSS *g-r-i* sequence, respectively. The images were subject to 2×2 binning and exposure times set at 30 s across both nights. Seeing varied typically from $1''$ to $2''.5$ across both nights, with conditions improving during the later half of the night for both runs.

Additional observations were collected by the robotic 0.6 m TRAPPIST-North (Jehin et al. 2011) on the nights of UT 2019 November 24–26. TRAPPIST-N is located at the Oukaimeden Observatory in the Atlas Mountains in Morocco. This telescope features an Andor iKON-L BEX2-DD CCD camera imaging through a Cousins *R* filter. Additional instrument specifications include a $0''.60 \text{ pixel}^{-1}$ scale and a $22'$ square field of view. The images were binned 2×2 with exposure times set at 120 s. Seeing for the first night was variable with median on-chip values ranging from $\sim 3''$ to $4''.2$, with conditions improving on the second night, where values were in the range of $\sim 2''.7$ – $4''$. The final night unfortunately presented poor observing conditions, so we refrained from using data from this night in our analysis.

Observations in 2021 corresponding to nights UT October 27–30, as well as one night in 2018 on UT November 04, were carried out at La Silla Observatory using the Danish 1.54 m telescope (labeled “Danish” in Table B3). The DFOSC instrument on this telescope has a deep depleted BI 2k \times 2k sensor with $13.5 \mu\text{m}$ square pixels, and we used it unbinned. Integration times were between 60 and 140 s, and the telescope was tracked at half the apparent rate of the asteroid, providing star and asteroid source profiles in one frame.

For the remaining observations from the 2018 apparition we used the Ondřejov Observatory 0.65 m telescope (labeled

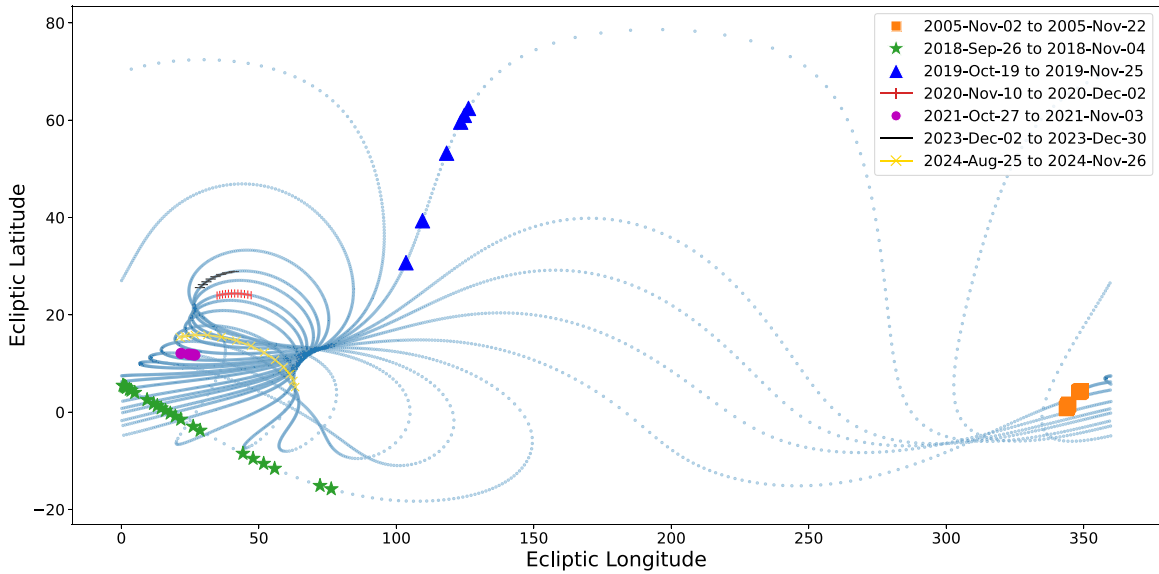


Figure 1. Geocentric ecliptic coordinates at the time observations of 2005 UD were obtained. The small blue circles indicate the ecliptic coordinate of 2005 UD from 2005 September 5 to 2024 December 31 with a resolution of 1 day. The 2005, 2018, 2019, and 2021 dense light curves included in our analysis are shown as the orange squares, green stars, blue triangles, and magenta circles, respectively. A past viewing opportunity in 2020 November is represented as the red vertical hash region. Additional viewing opportunities of 2005 UD in late 2023 and late 2024 are represented as the black horizontal ticks and yellow cross regions, respectively. Ecliptic coordinates of 2005 UD were obtained from JPL Horizons (Giorgini et al. 1996).

“Ondřejov” in Appendix B). The 0.65 m is a reflecting telescope operated jointly by the Astronomical Institute of ASCR and the Astronomical Institute of the Charles University of Prague, Czech Republic. It uses a Moravian Instruments G2-3200 MkII CCD camera (with a Kodak KAF-3200ME sensor and standard *BVRI* photometric filters) mounted at the prime focus. The CCD sensor has 2184×1472 square pixels ($6.8 \mu\text{m}$ pitch) with microlenses, and we imaged in 2×2 binning mode, providing $1''.05 \text{ pixel}^{-1}$ and a $19' \times 12'.8$ field of view. Integration times were between 30 and 100 s, and we set the tracking at half-apparent rate of the asteroid.

We sourced the sparse data from the following:

1. observations from the Catalina Sky Survey (CSS; Larson et al. 2003);
2. observations from the Pan-STARRS project (Chambers et al. 2016);
3. images from the ZTF project (Bellm et al. 2019) downloaded from the IRSA server (<https://irsa.ipac.caltech.edu/applications/ztf/>); and
4. observations from the ATLAS project (Tonry et al. 2018).

For all but the ZTF sparse data we utilized the calibrated chip-stage photometry (unpublished) and associated Julian dates reported on the Minor Planet Center (MPC).²¹ Processing of the ZTF images is described in the following paragraph.

We bias- and flat-field-corrected data from our new observations using standard techniques. We used the Python-based *PhotometryPipeline* (Mommert 2017) to measure the photometry of these new data, as well as the ZTF sparse data. We note that neither the field stars nor 2005 UD were trailed, and thus irregular photometry was not required for these new observations. A high-level overview of the pipeline workflow is as follows: astrometry using SCAMP (Bertin 2006), which utilizes the Vizier catalog service (Ochsenbein et al. 2000) to

perform image registration via the Gaia Data Release 2 catalog (Gaia Collaboration et al. 2018); point-source extraction using Source Extractor (Bertin & Arnouts 1996); photometric zero-point calibration using the Pan-STARRS DR1 catalog (Flewelling et al. 2020); and distilling the calibrated photometry by using the object’s position in the frame as returned through a query to the JPL Horizons system (Giorgini et al. 1996). Additionally, the pipeline executed photometric calibration using stars with solar-like colors in the same frame from the SDSS DR9 catalog (Ahn et al. 2012), where the color thresholds were set at $(g - r) = 0.44 \pm 0.2$ and $(r - i) = 0.11 \pm 0.2$. Using the curve-of-growth procedure outlined in Mommert (2017), the pipeline determined a best-fit aperture radius of 2.84–4.53 binned pixels ($1''.22''$ – $1''.94''$) for the NOT data and 3.26–5.37 binned pixels ($1''.17''$ – $1''.93''$) for the LDT data. The TRAPPIST data were the only exception to this, where we manually set apertures of 5-pixel radius ($3''$).

Data from the 2018 and 2021 apparition that were taken with the Ondřejov Observatory 0.65 m and Danish 1.54 m telescopes were subject to a custom aperture photometry program Aphot + Redlink developed by Petr Pravec and Miroslav Velen. In short, the software performs a semiautomated routine to select optimal apertures for the photometry. Star-like sources in the science frames are calibrated in the Johnson–Cousins *V–R* system with standard stars from Landolt (1992) facilitating 0.01 mag precision in photometric conditions.

Appendix B includes further details of all light curves used in our analysis. Figure 1 shows ecliptic coordinates corresponding to our new observations, as well as future apparitions.

3. Light Curve Inversion

Light curve inversion has been used to ascertain spin states of NEAs; see models for, e.g., Phaethon (Hanus et al. 2016; Hanuš et al. 2018), Cuyo (Rozek et al. 2019), and Apollo (Kaasalainen et al. 2007; Āurech et al. 2008). In addition to the necessity of good-quality data (i.e., high signal-to-noise ratio),

²¹ https://minorplanetcenter.net/db_search

a unique solution requires data obtained across a broad range of viewing geometries (i.e., sampling reflectance data from as much of the surface of the object as possible). To determine the shape (expressed as a convex polyhedron) and pole solution of 2005 UD, as well as refine its sidereal rotation period, we used the *convexinv* program, described in Kaasalainen & Torppa (2001) and Kaasalainen et al. (2001).

Prior to carrying out light curve inversion, we formatted the data (see the *convexinv* documentation) into standard “blocks.” We employed the *astropy*-affiliated (Tardioli et al. 2017) *astroquery* tool to obtain Sun and Earth xyz vector components, centered on 2005 UD and expressed in au, for each data point via the JPL Horizons service (Giorgini et al. 1996). Additionally, all light curves were normalized to unity and converted to flux units before correcting observation times for light-travel time. As a final step, all flux values were range-corrected to 1 au from the Earth and Sun.

Of the original light curve set from Devogèle et al. (2020), we discarded five light curves obtained at the Lowell Observatory 0.79 m National Undergraduate Research Observatory telescope (31in henceforth) and one light curve from TRAPPIST-N due to high photometric noise or having temporally overlapping data from a superior instrument (although our model light curves were able to reproduce these data). These six light curves correspond to observations on UT 2018 September 27, October 6, October 10, October 15, October 16, and October 17. Additionally, we exclude the first half of one LDT light curve from our new data taken on UT 2019 October 18 from the shape modeling procedure because light curve predictions from our best-fit shape models did not agree with the uncharacteristic 0.5 mag amplitude; the cause for the discrepancy in this light curve with our models is unknown. Preparing the sparse data sets included rejecting any data points taken near the magnitude limit of the specific instrument and plotting the observed intensities versus the associated phase angles and performing a sigma-clipping routine to eliminate outliers.

3.1. Rotational Period

To get a reliable shape solution, it is imperative to constrain the rotational period of the object. The parameter space is riddled with local minima due to the rotational period, which, since *convexinv* is a gradient-based algorithm, will cause the optimizer to get trapped and converge to an ill-fitting solution. The spacing of these local minima ΔP (in hours) in the period-space χ^2 spectrum is given roughly by $\Delta P \approx P^2/(2T)$, where P is the rotational period of the object and T is the time span of the entire data set (Kaasalainen et al. 2001). We ensured that the step size of the period search did not increase significantly above this value to prevent missing the correct period. We define a unique period or spin solution if its χ^2 (see Section 3.1 in Kaasalainen & Torppa 2001 for how this test statistic is calculated) is lower than that of all other candidate solutions by at least 10% (also used in Hanuš et al. 2011). Note that while the criterion employed in Hanuš et al. (2018) suggests that a χ^2 threshold of $\sim 5\%$ above the minimum is valid for our data set, we opt for the more rigorous 10% threshold to make the global minimum more distinct.

Prior to running *period_scan*, we specified a narrow period search window centered on the literature value and assigned weights to each light curve to improve the goodness of fit; noisy and sparse light curves were assigned lower weights. We

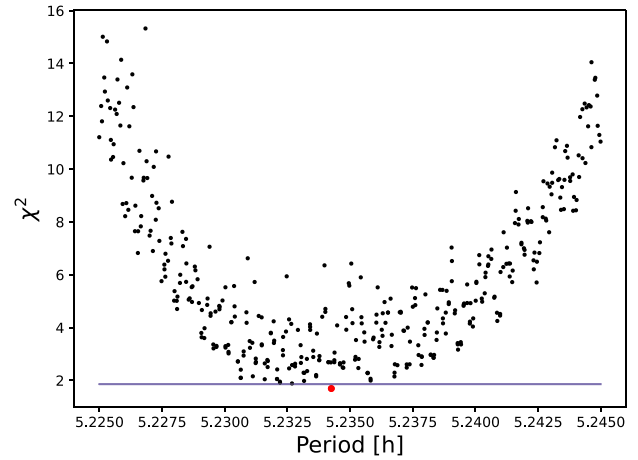


Figure 2. The *period_scan* results from our set of 84 light curves with optimized weights. The black points represent local minima in the sidereal period, pole orientation, and shape parameter space. The blue horizontal line shows the χ^2 value 10% higher than the global minimum to which we consider points underneath to be viable solutions. The only solution that satisfies this criterion for the rotational sidereal period with our data set is $P_{\text{sid}} = 5.234246 \pm 0.000097$, shown in red.

optimized the individual weights W_{LC} for each remaining dense light curve quantitatively using $W_{\text{LC}} = 1/\text{rms}^2$, where the rms error is obtained by fitting a Fourier series to each light curve. Next, all nonzero weights for dense light curves were then multiplied by a scale factor to bring the sum of the dense light curve weights equal to the number of nonrejected dense light curves (in our case 78). For the 2005, 2019, and 2021 apparitions we fit a Fourier series up to the seventh order to each light curve. For the 2018 apparition, we limited the fitted Fourier series to second order as a form of regularization since these 2018 data compose $\sim 80\%$ of our dense light curves. Performing various shape modeling trials showed that fully optimizing the weights for all dense light curves biased the model heavily to the 2018 apparition by suppressing the weights of the light curves from the other apparitions. This is likely because data from the other apparitions, particularly from 2005 and 2021, are quite limited in both quantity and quality. Further, because of 2005 UD’s relatively smooth and invariant sinusoidal light curve (see Figure 5 for an example), we determined that a second-order Fourier series was sufficient in penalizing lower-quality light curves without significantly underestimating the weights of the high-quality ones. For the sparse light curves, we assign weights at the 10% or 20% level (see Section 3.2) by taking the average of the lowest 10% or 20% of weights of the dense light curves.

The *period_scan* results within a search range of 5.225 and 5.245 hr produced a unique sidereal rotational period value of $P_{\text{sid}} = 5.234246 \pm 0.000097$ hr (Figure 2). A comparison of our period solution with those from previous studies is presented in Table 1. A previous period search for 2005 UD conducted in Devogèle et al. (2020) suggested the possibility of a three-peaked light curve corresponding to a rotation period around 7.85 hr. With the addition of our new data, we note significant reduction in the goodness of fit for periods in this vicinity. As such, we can now exclude sidereal period solutions in this range and surmise that this is an alias.

Table 1
Comparison of Previous Rotational Period Estimates for 2005 UD with This Work

Period (hr)	Uncertainty (hr)	Source
5.23		Jewitt & Hsieh (2006)
5.2492		Kinoshita et al. (2007)
5.231	± 0.034	Sonka et al. (2019)
5.235	± 0.005	Devogèle et al. (2020)
5.2340	$\begin{smallmatrix} +0.00004 \\ -0.00001 \end{smallmatrix}$	Huang et al. (2021)
5.234246	± 0.000097	This work

3.2. Spin and Shape Solutions

Using our period solution, we followed the standard *convxinv* recipe to derive a shape model. We specified 48 initial pole orientations isotropically distributed on the celestial sphere at 30° spacing, which is later optimized during the inversion procedure. The uncertainties for the sparse data from the MPC (all but the ZTF data) are not reported. Thus, the contribution of each sparse data set toward convergence was assessed by performing a coarse grid search across all sparse data combinations, where each individual sparse light curve was assigned a 0%, 10%, or 20% weight. By scanning through these weights, we aimed to minimize the relative χ^2 value for the dense light curves only. Following this test, we assigned a weight of 10% to all but the ZTF data (assigned 20%), as this specific combination produced the lowest χ^2 . This combination is not surprising since we reduced the ZTF sparse data ourselves and thus had the knowledge to reject individual data points based on error, source blending, etc. The ZTF data also had the largest phase-angle coverage (i.e., more viewing geometries) of the sparse data sets, covering $\sim 100^\circ$ in phase over a 3 yr span.

Following this, we were left with four probable spin solutions, which are listed in Table 2. All four shape models had a small dark facet area (below 1% of the total facet area), which is needed to preserve convexity, so we were not able to eliminate any of these candidate solutions using this metric. Further, this suggests that nonconvex features (e.g., concavities) do not occupy a significant area on 2005 UD’s surface. Following this, we computed the inertia tensors (see Dobrovolskis 1996 for a full description) of the shape models to discover that Solution 1 and Solution 4 had an inertial axis significantly misaligned from the z -axis, so we rejected these solutions on the basis of being nonphysical (i.e., there is no evidence that 2005 UD is in nonprincipal axis rotation). However, one caveat is that if 2005 UD is not uniform in color (see Section 4.1) or density, then our convex approximation may contain systematic errors that could manifest as the aforementioned inertial axis misalignment.

This left us with Solution 2, $(\lambda_2, \beta_2) = (116^\circ.6 \pm 2^\circ.2, -53^\circ.6 \pm 4^\circ.7)$, and Solution 3, $(\lambda_3, \beta_3) = (300^\circ.3 \pm 2^\circ.5 - 55^\circ.4 \pm 2^\circ.2)$ (1σ errors), which are equally well fitting. Errors were estimated by agitating various parameters during dozens of trial runs and investigating the effects on χ^2 values. Solution 3 is interesting because constraints on the pole orientation of (3200) Phaethon place it in the range of $308^\circ \lesssim \lambda \lesssim 322^\circ$ and $-40^\circ \lesssim \beta \lesssim -52^\circ$ (Kim et al. 2018 and Hanuš et al. 2018), which is within our 3σ error. Further discussion on the implications of these pole solutions for the formation of 2005 UD is given in Section 5.

Table 2
Candidate Spin Solutions after Performing Light Curve Inversion

Solutions	λ (deg)	β (deg)	χ^2	rms
1 ^a	144.0	-31.8	3.0542	0.0202
2	116.6	-53.6	3.1037	0.0203
3	300.3	-55.4	3.1190	0.0204
4 ^a	62.5	-44.2	3.2048	0.0207

Note.

^a Rejected due to nonphysical shape. χ^2 and rms quantify fits to dense light curves only.

Recent shape modeling efforts using the Lommel–Seeliger ellipsoid method by Huang et al. (2021) yielded two candidate pole solutions for 2005 UD: (1) $(72^\circ.6^{+4.2}_{-7.3}, -84^\circ.6^{+6.2}_{-2.1})$ and (2) $(285^\circ.8^{+1.1}_{-5.3}, -25^\circ.8^{+5.3}_{-12.5})$. Pole 2 is favored as their preferred solution and is both comparable to Phaethon’s and largely in agreement with our Solution 3 with overlap in longitude within 3σ errors.

Thermal data of 2005 UD from two different epochs were obtained during the Near-Earth Object Wide Infrared Explorer (NEOWISE) reactivation mission (Mainzer et al. 2014) using the two shortwave filters (W1: $3.1 \mu\text{m}$; W2: $4.6 \mu\text{m}$). Thermophysical modeling of these data was presented in Devogèle et al. (2020). The best-fit solution from the thermophysical model ($\lambda_{\text{TPM}} = 102^\circ \pm 20^\circ$ and $\beta_{\text{TPM}} = -35^\circ \pm 30^\circ$) is consistent with Solution 2. Given that the other pole solution candidates (Solutions 1, 3, and 4) were inconsistent with the predicted longitude from the thermophysical analysis and Solution 2 consistently attained the lower χ^2 among numerous trial runs, we adopt $\lambda_p = 116^\circ.6 \pm 2^\circ.3$, $\beta_p = -53^\circ.6 \pm 5^\circ.4$ as our preferred solution. A comparison between our pole solutions from light curve inversion, solutions from the above thermophysical modeling, and Phaethon’s pole is illustrated in Figure 3.

The convex shape (Figure 4) from our preferred pole solution $(\lambda_p, \beta_p) = (116^\circ.6, -53^\circ.6)$ is nearly identical to our other candidate solution $(\lambda, \beta) = (300^\circ.3, -55^\circ.4)$. This is expected because there remains a 180° ambiguity in ecliptic longitude for the two solutions for roughly the same pole latitude. We thus expect features to be mirrored across the x - z plane. As an additional test in the validity of these two solutions, we computed light curve predictions of these two shapes and analyzed them by eye to find equally good agreement with all of our light curves. A suite of 12 plots illustrating the fits between synthetic and real light curves from epochs in 2005, 2018, 2019, and 2021 using our preferred solution is shown in Figure 5.

4. Current State of Knowledge of 2005 UD Physical Properties

For reference, we provide a master summary of known properties for 2005 UD in Table A1.

4.1. Albedo, Size, and Shape

Thermal emission observations, coupled with photometry, are of particular value for albedo and size determination. A thermophysical study of 2005 UD by Masiero et al. (2019) presented a value of 0.14 ± 0.09 for the geometric albedo and 1.2 ± 0.4 km for the effective diameter. However, Masiero

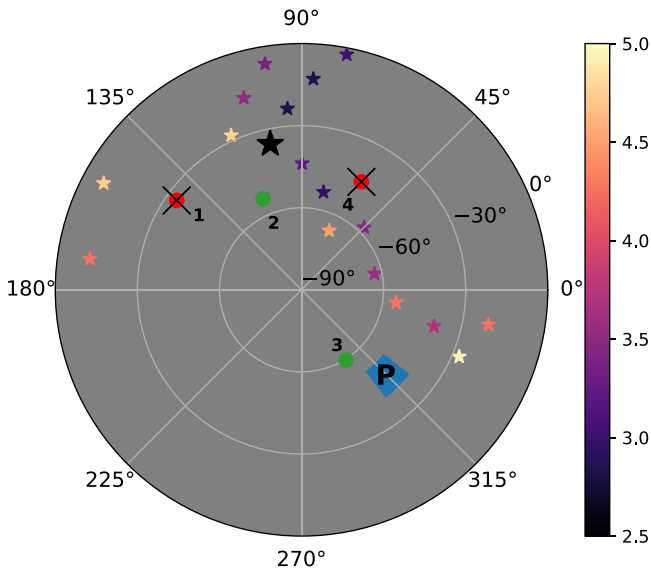


Figure 3. Polar projection map comparing our four pole solutions from light curve inversion, candidate thermophysical pole solutions from Devogèle et al. (2020), and Phaethon’s spin pole region from Hanuš et al. (2018) and Kim et al. (2018). The map is centered on the south ecliptic pole. The green circles show accepted light curve inversion solutions, while the crossed-out red circles represent our rejected solutions. The color bar represents χ^2 values of the thermophysical solutions, which are represented as stars; only retrograde solutions with $\chi^2 \leq 5$ are shown for clarity. The best-fitting thermophysical solution is represented by the large black star. Phaethon’s spin axis orientation with approximate uncertainty is marked as the letter *P* surrounded by the blue extended region.

et al. (2019) note that the modeling was only based on data from two observational epochs from the NEOWISE survey.

The most recent values to be reported come from Devogèle et al. (2020), with an effective diameter of 1.3 ± 0.2 km and geometric albedo of 0.10 ± 0.02 based on photometry and an albedo–polarimetry relation (Cellino et al. 2015). Devogèle et al. (2020) also included thermophysical modeling (using a different technique from that used in Masiero et al. 2019) to derive a geometric albedo of 0.14 ± 0.07 and effective diameter of $1.12^{+0.49}_{-0.21}$ from the same limited NEOWISE data set. Despite the slight differences in these nominal values, they are all consistent and suggest that the albedo and diameter of 2005 UD are well constrained.

Our shape models of 2005 UD reveal that the general shape can be inferred as a triaxial ellipsoid with $a/b = 1.41$ axis ratio that produces symmetric sinusoidal light curves with amplitude of about 0.4 mag. We notice prominent flat areas at the north and south poles on our convex shape approximation, which is expected, as these areas are the least constrained with unresolved disk-integrated photometry. Devogèle et al. (2020) is the only other work to have attempted shape modeling of 2005 UD using our methods (as presented in Kaasalainen et al. 2001), and they showed that their light curve data alone could not eliminate the possibility of a sidereal period of ~ 7.85 hr. With the addition of our new data, the possibility of a three-peaked light curve and consequently a shape more akin to a tetrahedron is nonviable.

4.2. Surface Colors

We analyzed a time series of photometric colors of 2005 UD derived from 341×30 s exposures taken in a $g-r-i$ sequence at the NOT (Section 2.1) to investigate previously reported

variations in surface color (Kinoshita et al. 2007). These multifilter light curves span one complete rotation of the body. Calibrated photometry using the Aperture Photometry Tool (APT; Laher et al. 2012) shows the following apparent magnitudes: $g = 19.34 \pm 0.01$, $r = 18.87 \pm 0.01$, and $i = 18.80 \pm 0.01$. We thus report colors as $(g - r) = 0.47 \pm 0.01$ and $(r - i) = 0.07 \pm 0.01$. To compare with Johnson–Cousins colors of 2005 UD from prior analyses, we performed color transformations using $(B - g)$, $(V - g)$, $(R - r)$, and $(R - I)$ equations from Jordi et al. (2006). Our results are consistent with previous works and are displayed in Table 3.

To check for rotational color variability, we computed color as a function of rotation by linearly interpolating between adjacent points, e.g., measured g minus interpolated r (Figure 6). Within the signal-to-noise ratio of our data we did not detect any systematic color variations that are more significant than 1σ away from the mean across the region of the body visible during this observation period. This null detection is consistent with the results of (1) Devogèle et al. (2020), who used separate spectroscopic and polarimetric methods to probe for surface heterogeneity, and (2) Kareta et al. (2021), who saw no color variations in the near-infrared.

Our above-mentioned results are in contrast to Kinoshita et al. (2007), who reported ~ 0.2 mag $R - I$ color variation. One explanation for this discrepancy is that 2005 UD’s surface color differs as a function of latitude, as there was a $\sim 52^\circ$ difference in the subobserver ecliptic latitudes accessed by these two color data sets. This modest difference in subobserver latitude suggests that any color heterogeneity on the surface would have to be confined to small ($< 50^\circ$ in latitude) yet highly contrasting spots in order to have an influence on the hemispherical averages represented by unresolved, ground-based photometry. Photometric modeling of such a spotted surface could provide insight on whether this interpretation is physically plausible, but this is beyond the scope of this work. Notably, a recent study by MacLennan et al. (2022) found evidence that Phaethon’s surface is heterogeneous as a function of latitude, which adds merit to the above hypothesis. Future multicolor photometric observations could provide further insight into 2005 UD’s surface properties.

4.3. Activity and Dust Production Limits

Given the detection of activity associated with Phaethon, we conducted a search for indications of a faint coma or dust tail around 2005 UD. We utilized the image processing tool Siril²² to stack LDT images from the night of 2019 November 18 using an average combination procedure with no rejection (Figure 7). The stacked image corresponds to 10,910 s (about 3 hr) of integration time with a calculated depth of 26.8 mag arcsec⁻² within an annulus extending $\theta = 1''.8 - 3''.6$ from the object center; this is the deepest existing stacked image of 2005 UD at the time of writing. We used the APT (Laher et al. 2012) to measure a radial surface brightness profile to compare this stacked image of 2005 UD with a close field star to search for indications of a faint coma. We then fit the model

$$S(r) = A + Br + Cr^2 + Dr^3 + Er^4 + Fe^{-\frac{r^2}{2\sigma}},$$

which is explained in Laher et al. (2012). Next, we subtracted the background levels from the profiles and associated models

²² <https://www.siril.org/>

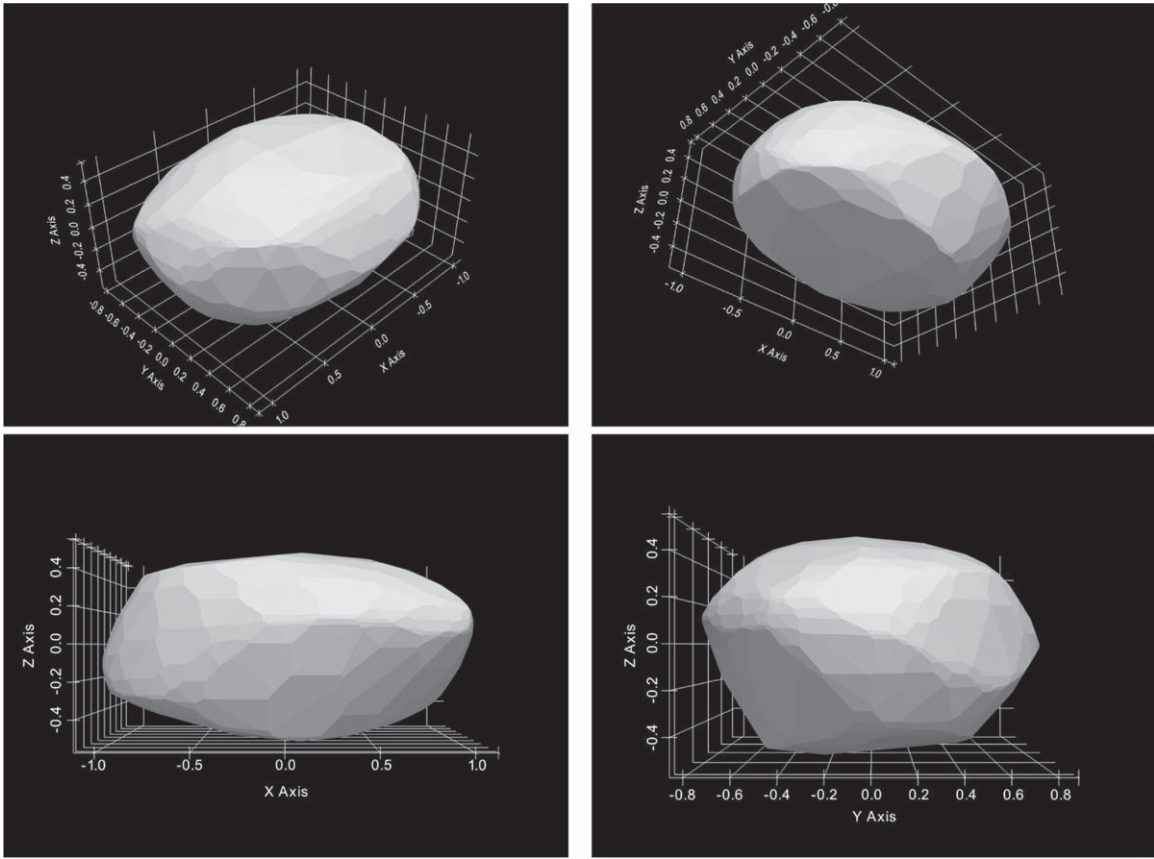


Figure 4. Convex shape model of 2005 UD using our preferred pole solution displayed in a variety of viewing geometries. View descriptions in left to right progression: positive isometric, negative isometric, along y -axis, and along x -axis. The scale values are unitless and show the relative sizes of the xyz -axes of our convex approximation. The equator of 2005 UD is parallel to the x - y plane. The light source was arbitrarily placed and does not necessarily reflect the location of the Sun for any given observation.

before normalizing the field star radial profile to the peak flux of the stacked 2005 UD profile. The results of these efforts are showcased in Figure 7 alongside a similar analysis performed on the active Centaur 2014 OG392 from Chandler et al. (2020) for comparison.

An additional quantitative search for a faint dust stream or tail was performed by analyzing summed pixel values in annular slices around the stacked asteroid (as demonstrated in Chandler et al. 2021) to search for excess flux in the anti-solar and anti-motion direction. Along with visual scrutiny, no indications of activity from 2005 UD were detected. Importantly, if 2005 UD exhibits activity via thermal fracturing of the surface regolith (akin to Phaethon), we would expect difficult detection circumstances (Ye et al. 2021) because 2005 UD was close to aphelion (heliocentric distance of 1.7 au) at the time these data were gathered. Targeted observations of 2005 UD near perihelion might offer a better chance at detecting activity.

One way to place an upper limit on mass loss is by using a simple model with knowledge of the limiting magnitude within a projected annulus. We again used the stacked image from the LDT for this procedure using an annulus of size $\theta = 1''.8-3''.6$. Using the procedure outlined in Section 3.2 of Jewitt (2013), we derive an upper limit of either 0.37 kg s^{-1} or 0.04 kg s^{-1} based on assumed grain radii of 10 mm (the upper limit of surface grain size from Devogèle et al. 2020) and $1 \mu\text{m}$, respectively. Additionally, we assume a material density of 1500 kg m^{-3} . Following Jewitt (2013), we use particle ejection velocities of 1 m s^{-1} for millimeter-sized grains and 1 km s^{-1}

for micron-sized grains. These upper limit results are largely consistent with the $\lesssim 0.1 \text{ kg s}^{-1}$ estimate derived by Kasuga & Masiero (2022) using NEOWISE observations.

5. A Common Origin with Phaethon?

With additional data from new viewing geometries, we were able to constrain two possible spin solutions for 2005 UD: $(\lambda_p = 116^\circ.6, \beta_p = -53^\circ.6)$ and $(\lambda = 300^\circ.3, \beta = -55^\circ.4)$. Whether the presence of a mirror solution is a consequence of 2005 UD's unusual orbit or by coincidence is not exactly known. Observations of 2005 UD during upcoming apparitions may yield further information from more viewing geometries so as to further constrain a single pole solution; Figure 1 displays both past and upcoming viewing geometries that will be accessible in the next few years. The plausibility and implications for formation for each pole solution are discussed in the next section.

5.1. Comparing Pole Solutions

An intriguing result to come out of our analysis is a well-fitting pole solution that is consistent with Phaethon's in both longitude and latitude (see Section 3.2). This encourages a formation scenario where 2005 UD separates from parent body Phaethon under a mechanism that does not disturb the spin vector. Formation via Yarkovsky–O'Keefe–Radzievskii–Paddack (YORP) spin-up (Rubincam 2000) is one such possible formation mechanism for the Phaethon–2005 UD pair.

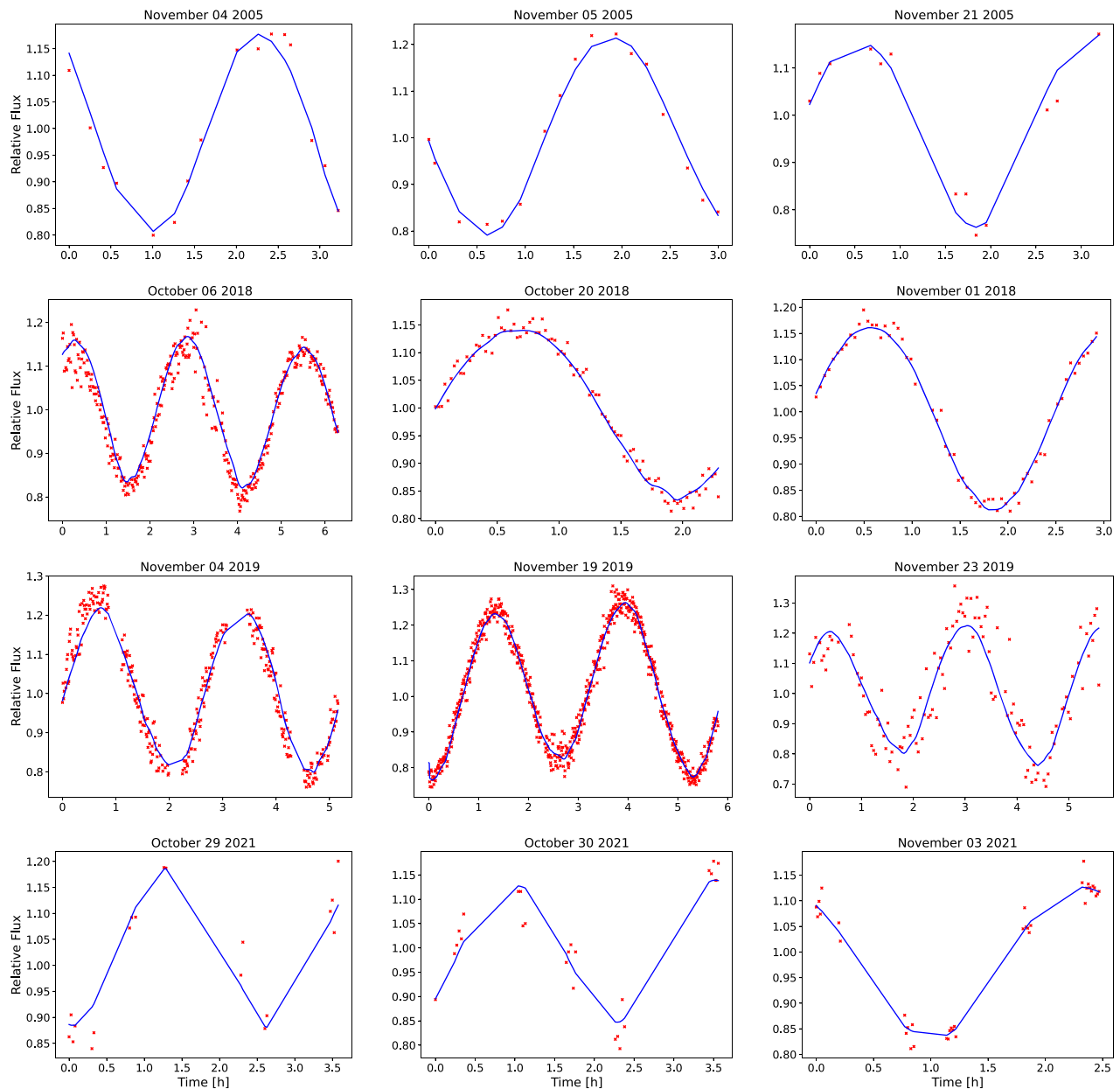


Figure 5. Suite of 2005 UD light curves compared to model fits. Each plot features a single light curve from assorted epochs in 2005, 2018, 2019, and 2021. Overlaid are light curve predictions of our preferred model from the convex inversion procedure represented as a solid blue line. UT dates marking the start of observations for each light curve are present as plot titles. The data behind this figure are available and include all 84 individual observations; see tables in Appendix B for details on each observation. The data are in the form of a DAMIT input file. User can run the code to get the model values or extract the observed, relative brightness from the input file.

(The data used to create this figure are available.)

Certainly this is a common mechanism for the formation of most known asteroid pair systems (Pravec et al. 2010), and interestingly, both the convex approximation of Phaethon from Hanuš et al. (2018) and the radar shape model from MacLennan et al. (2022) suggest the existence of an equatorial ridge and top-like shape, characteristic of YORPoids (Ostro et al. 2006; Busch et al. 2011; Naidu et al. 2015). Under a YORP-induced, post-fission scenario, 2005 UD and Phaethon would have engaged in a protobinary state before disruption, eventually evolving into the unbound asteroid pair seen today (Jacobson & Scheeres 2011). Due to the complexity of this process and uncertainties regarding the mass distribution and

morphology of both Phaethon and 2005 UD, it remains unclear whether aligned poles are expected and/or consistent with a YORP spin-up scenario. Conversely, Pravec et al. (2019) found that current pole orientations of asteroids in a paired system generally do not reflect the original orientations at the time of separation, possibly due to solar torques (Breiter et al. 2005), YORP effects, and/or planetary encounters. For Phaethon (and possibly 2005 UD), the added dynamical effects of devolatilization add more uncertainty on how pole orientations would be affected (discussed more below). In the case of our preferred solution, which only shares a common ecliptic latitude with Phaethon, we do not consider pole realignment

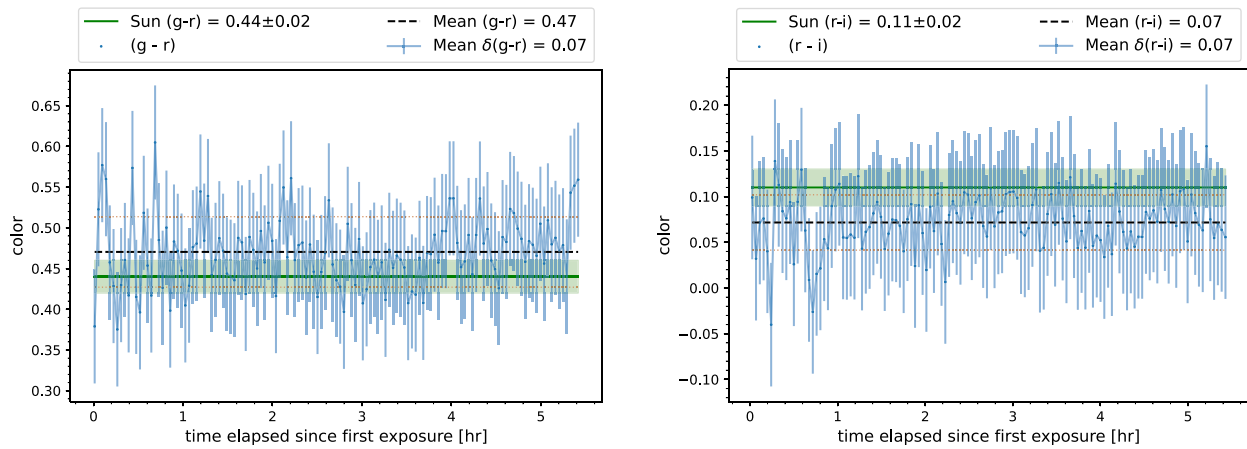


Figure 6. Left: $(g - r)$ color as a function of rotation. The data points were computed by subtracting linearly interpolated r from measured g for a given r - g - r sequence. The calculated mean of these residuals is shown as the dashed horizontal black line. We represent one standard deviation from the mean as the dotted horizontal red lines, which confirm no signs of color variation outside of this limit. The $(g - r)$ color of the Sun is underlaid as the green horizontal line with surrounding error for reference. Right: same as the left panel, but with $(r - i)$ color.

Table 3
Mean Surface Colors of 2005 UD and Phaethon

Body	$B-V$	$V-R$	$R-I$	References
2005 UD	0.65 ± 0.02	0.32 ± 0.01	0.32 ± 0.02	1
2005 UD	0.63 ± 0.01	0.34 ± 0.01	0.30 ± 0.01	2
2005 UD	0.66 ± 0.02	0.35 ± 0.02	0.33 ± 0.02	3
Phaethon	0.64 ± 0.02	0.31 ± 0.02	0.31 ± 0.03	4
Phaethon	0.61 ± 0.01	0.34 ± 0.03	0.31 ± 0.03	5
Phaethon	0.59 ± 0.01	0.35 ± 0.01	0.32 ± 0.01	6
Phaethon	...	0.34	...	7

References. (1) this work; (2) Kinoshita et al. 2007; (3) Jewitt & Hsieh 2006; (4) Lee et al. 2019; (5) Kasuga & Jewitt 2008; (6) Dundon 2005; (7) Skiff et al. 1996.

due to planetary flybys a likely scenario because the minimum orbital intersection distance (MOID) value for both bodies is too high for all planets. YORP ultimately may also be invalid here due to the proposed recent separation of less than 100 kyr (Hanus̄ et al. 2016; MacLennan et al. 2021), which is much shorter than the tens of millions of years required for significant changes due to YORP (Rubincam 2000). To probe the extent to which current-day spin poles for 2005 UD and Phaethon line up or differ as a result of any of these physical process would require detailed modeling beyond the scope of this paper.

Due to Phaethon’s rare status as an active asteroid, volatile-driven separation is another possible formation mechanism for this pair. This conjecture, however, does not rule out rotational fission entirely since induced torques due to outgassing cause spin changes in comets (Steckloff & Jacobson 2016). Akin to similar processes responsible for cometary splitting (see Jewitt 2021 and references therein), episodes of activity in an ancestor body could have worked, perhaps in concert with YORP, to accelerate the body to its critical spin rate, resulting in fission. However, the fact that 2005 UD is clearly in a principal axis rotation state (i.e., it is not tumbling) may speak to a more ordered scenario of formation that did not involve processes, like volatile-driven outgassing, that can produce nonprincipal axis rotation. Damping time estimates using Equation (11) in Pravec et al. (2014) of a nonprincipal axis rotator of 2005 UD’s size and rotation exceed the proposed age

of this system by millions of years, further suggesting that a chaotic, purely volatile-driven splitting event was unlikely.

Based on our results and arguments presented above, we lean toward a common origin due to a YORP fission scenario being the most likely progenitor for the 2005 UD–Phaethon cluster. This interpretation is consistent with that made by Huang et al. (2021), who also presented a Phaethon-like pole solution for 2005 UD using a different method. We encourage modeling of this specific sequence of events to probe the effects on spin pole in such a scenario.

5.2. Nongravitational Influences

The Yarkovsky effect (Bottke et al. 2006) is relevant when considering nongravitational perturbations for small (generally less than ~ 10 km diameter) bodies. In general, a secular decrease in semimajor axis is expected for retrograde rotators (as opposed to outward drift for prograde rotators) such as Phaethon and 2005 UD. 2005 UD is approximately one-fifth the size of Phaethon, which would subject it to more rapid inward drift in semimajor axis. However, the semimajor axis of 2005 UD is currently greater by $\sim 3.5 \times 10^{-3}$ au than that of Phaethon, and dynamical integrations (Ohtsuka et al. 2006) suggest that that has been the case for thousands of years. Furthermore, the presumed recent (< 100 kyr ago) separation of this pair means that the Yarkovsky effect has not had enough time to significantly alter these objects’ orbits. Typical Yarkovsky drift rates of 10^{-4} au Myr $^{-1}$ for kilometer-scale bodies suggest that ~ 10 Myr would be needed to explain their current difference in semimajor axis, and that does not account for any time associated with a necessary change in pole orientation (e.g., by the YORP effect) that would allow for Yarkovsky drift to be in the right direction. It is additionally unlikely that the current low levels of activity seen for Phaethon play any significant role in the orbital dynamics of the system, though prior epochs with higher levels of activity may have contributed to the present-day separation.

If Phaethon and 2005 UD did in fact separate recently, it is suggested (MacLennan et al. 2021) that orbital dynamics governed by interactions with the terrestrial planets remain the most plausible dynamical pathway to produce the configuration of orbital elements we see today. However, a definitive time line associated with a separation event between Phaethon and

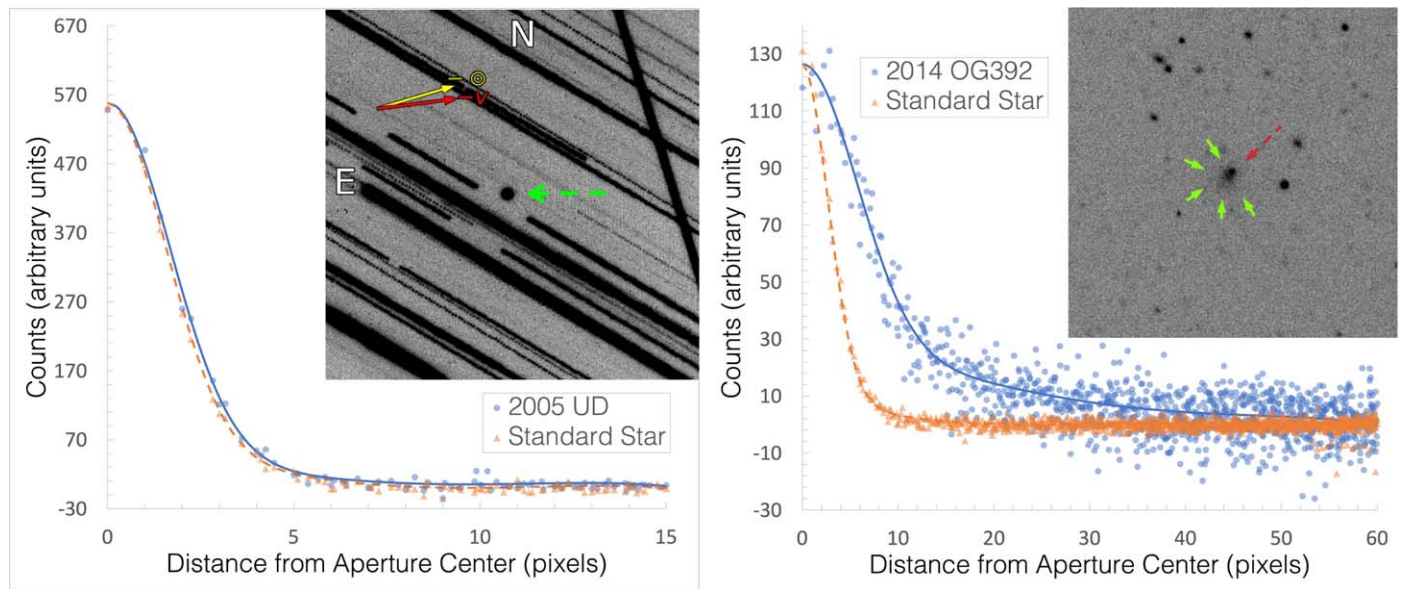


Figure 7. Left: radial surface brightness profiles of 2005 UD and a nearby field star in an LDT stacked image from UT 2019 November 18. We see no indication of extended emission or faint activity. The stacked image of the asteroid corresponds to $\sim 10,960$ s (about 3 hr) of integration time and reaches a limiting magnitude of about $26.8 \text{ mag arcsec}^{-2}$. The stellar profile we measured was from a single 16 s exposure, and we normalized it to the peak of the stacked asteroid profile to facilitate comparison. Right: similar plot from Chandler et al. (2020) featuring active Centaur C/2014 OG392 (Pan-STARRS) to demonstrate the profile structure for an active object (reproduced with permission from the authors).

2005 UD has yet to come to fruition. We hope that improved orbit solutions and physical evidence of a fission-type disruption event following the DESTINY+ flyby could provide more insight into this issue.

Lastly, it is worth mentioning that (225416) 1999 YC is a putative third component in the 2005 UD–Phaethon system (Kasuga & Jewitt 2008; Ohtsuka et al. 2008). The addition of this body to the system supports a rotational fission formation scenario (Hanuš et al. 2018), but a spectral type inconsistent with the other two bodies (Kasuga & Jewitt 2008) and a significantly larger semimajor axis are hard to reconcile with any common origin theory.

Given these considerations, it seems unlikely that nongravitational forces would have played an important role in any evolution of 2005 UD relative to Phaethon. This does not necessarily influence arguments in favor of or against these two objects sharing a common origin.

6. Summary and Future Work

We conducted observations of 2005 UD during its recent apparitions in 2018, 2019, and 2021 using six different telescopes (4.3 m LDT, 2.6 m NOT, Danish 1.54 m, Ondřejov 0.65 m, and 0.6 m TRAPPIST-North and TRAPPIST-South) motivated by a fortuitous opportunity to collect data at new aspect angles. Our goals for this analysis included finding a unique sidereal rotational period, pole solution, and thus an accurate shape for 2005 UD by means of light curve inversion. We supplemented these data with archival dense and sparse light curves from epochs in 2005–2021 prior to performing light curve inversion. We presented a refined sidereal rotational period of $P_{\text{sid}} = 5.234246 \pm 0.000097$ hr. We conclude that 2005 UD has two equally well-fitting spin solutions given as $(\lambda_p = 116^\circ.6, \beta_p = -53^\circ.6)$ and $(\lambda = 300^\circ.3, \beta = -55^\circ.4)$, the former having preference considering the proximity of all other candidate solutions from our extensive light curve inversion trials and thermophysical modeling results from

Devogèle et al. (2020). Furthermore, the preferred solution from Huang et al. (2021) of $(285^\circ 8_{-5.1}^{+1.1}, -25^\circ 8_{12.5}^{+5.3})$ is only consistent in latitude with the latter of our two solutions given 3σ errors. Additional light curve data of 2005 UD from more viewing geometries may be needed to further constrain a unique spin solution and/or resolve inconsistencies with earlier studies. We thus encourage follow-up observations in upcoming apparitions to either help solve this problem or confirm our results (see Figure 1).

An activity search using the deepest stacked image of 2005 UD at the time of writing revealed no presence of dust production at orbital longitudes near aphelion. A simple model was used to infer an upper limit to mass loss of around $0.04\text{--}0.37 \text{ kg s}^{-1}$ depending on assumed grain size. This analysis should be applied to images of 2005 UD taken at or very close to perihelion to provide further constraints on the possibility of mass loss when surface temperatures are highest.

We analyzed time-series color data of 2005 UD over a full rotation and found no significant indications of surface color heterogeneity in Sloan $g\text{-}r\text{-}i$ bands. Understanding of the link between 2005 UD and Phaethon could be enhanced with additional searches for color heterogeneity, as the results presented in Section 4.1 are in contrast to those presented in Kinoshita et al. (2007) but are consistent with two other studies (Devogèle et al. 2020; Karetta et al. 2021). Additionally, there would be value to investigating the size of a patch of surface material that would be needed to result in detectable color variation on a body the size and shape of 2005 UD. This could be done, for example, through radiative transfer models or laboratory experiments.

Our secondary spin solution is aligned with Phaethon’s within error, which strengthens certain common origin scenarios. One such possibility is recent separation of 2005 UD and Phaethon in a YORP-induced fission event with conservation of angular momentum keeping the poles more or less aligned. However, the extent to which a parent body’s spin pole orientation would be preserved between separated pieces

in this circumstance is currently a question that is unable to be definitively answered. Phaethon’s perihelion-driven activity complicates this thought experiment, but present-day activity episodes reveal that they may not be intense enough (Jewitt & Li 2010; Li & Jewitt 2013) to have any real effect on spin axis. As such, we encourage efforts to model such scenarios.

Our spin solutions for 2005 UD spark interesting implications for orbital evolution via Yarkovsky forces. Current estimates for the age of the Phaethon cluster (assuming that they are genetically related) suggest that the Yarkovsky effect alone could not have resulted in the currently observed separation of members. While Ohtsuka et al. (2006) suggest dynamics consistent with a common origin, most recently Ryabova et al. (2019) performed backward orbital integrations spanning 5000 yr and concluded that 2005 UD and Phaethon do not share a common origin. It is, however, worth noting that dynamical analyses for 2005 UD have thus far neglected consideration of Yarkovsky and cometary forces, which could have a significant effect on the system dynamics. Although the presented spin solutions of 2005 UD may help to offer clues on its ancestry, more data and a better understanding of its detailed orbital dynamics are required to fully understand the origin of this unusual object.

We would like to thank the anonymous reviewers, whose feedback improved the quality of this manuscript markedly.

Support from Michael Mommert on the *PhotometryPipeline* simplified data processing steps during critical phases of this project. Matthew Knight offered helpful guidance on the mass-loss modeling work in this project. We would like to give thanks to Northern Arizona University’s HABLlab research group, Prof. Tyler Robinson, and Prof. Chadwick Trujillo for comments and suggestions that improved this work greatly.

The data presented here were obtained (in part) with ALFOOSC, which is provided by the Instituto de Astrofísica de Andalucía (IAA) under a joint agreement with the University of Copenhagen and NOT.

This work is based on observations made with the Nordic Optical Telescope, owned in collaboration by the University of Turku and Aarhus University and operated jointly by Aarhus University, the University of Turku, and the University of Oslo, representing Denmark, Finland, and Norway, respectively; the University of Iceland; and Stockholm University, at the

Observatorio del Roque de los Muchachos, La Palma, Spain, of the Instituto de Astrofísica de Canarias.

The work at Ondřejov Observatory, the work at the Danish 1.54 m telescope on the ESO La Silla station, and the work of J. H. were supported by the Grant Agency of the Czech Republic, grant 20-04431S.

TRAPPIST is funded by the Belgian Fund for Scientific Research (Fond National de la Recherche Scientifique, FNRS) under the grant PDR T.0120.21. TRAPPIST-North is a project funded by the University of Liège, in collaboration with the Cadi Ayyad University of Marrakech (Morocco). E.J. is F.R.S.-FNRS Senior Research Associate.

This material is based on work supported by the National Science Foundation Graduate Research Fellowship Program under grant Nos. 2020303693 and 2018258765. Any opinions, findings, and conclusions or recommendations expressed in this material are those of the author(s) and do not necessarily reflect the views of the National Science Foundation.

J.K. and N.M. acknowledge support from NASA Hayabusa2 participating scientist grant NNX16AK68G. J.K., N.M., and M.D. acknowledge support from NASA NEOO grant NNX17AH06G awarded in support of the Mission Accessible Near-Earth Object Survey (MANOS).

M.G., L.S., and G.F. acknowledge support from the Academy of Finland.

C.K. acknowledges support by the Swiss National Science Foundation under grant 185692.

S.M. acknowledges support from the Magnus Ehrnrooth Foundation and the Vilho, Yrjö, and Kalle Väisälä Foundation.

This research has made use of data and/or services provided by the International Astronomical Union’s Minor Planet Center. This research has made use of NASA’s Astrophysics Data System. This research has made use of SAO Image DS9, developed by Smithsonian Astrophysical Observatory (Joye & Mandel 2003). This work made use of the Lowell Observatory Asteroid Orbit Database *astorbDB* (Moskovitz et al. 2022). This work made use of the *astropy* (Astropy Collaboration et al. 2013) and SciPy (SciPy 1.0 Contributors et al. 2020) software packages.

Appendix A Master Summary Table for 2005 UD

Table A1 encompasses current known physical parameters for 2005 UD which we include for reference.

Table A1
2005 UD Physical Parameters

Parameter	Value	Reference
Discovery date	2005-Oct-22	MPEC 2005-U22
Discovery observer	E. J. Christensen	MPEC 2005-U22
Discovery survey	Catalina Sky Survey	MPEC 2005-U22
Orbital Elements		
Orbit type	NEA	NASA JPL Horizons
Family	Apollo	NASA JPL Horizons
Perihelion	0.1627 au	NASA JPL Horizons
Aphelion	2.3867 au	NASA JPL Horizons
Semimajor axis	1.2747 au	NASA JPL Horizons
Orbital inclination	28°6677	NASA JPL Horizons
Mean anomaly	90°7904	NASA JPL Horizons
Argument peri.	207°597	NASA JPL Horizons
Eccentricity	0.8723	NASA JPL Horizons
Long. ascending	19°7247	NASA JPL Horizons
T_J	4.507	NASA JPL Horizons
Orbital period	1.44 yr	NASA JPL Horizons
Spectroscopy		
Taxonomy (Bus –DeMeo)	B-type	Devogèle et al. (2020)
Spectral slope (Optical)	20% ± 10% μm^{-1}	Devogèle et al. (2020)
Spectral slope (NIR)	6% ± 1% μm^{-1}	Kareta et al. (2021)
Photometry		
Slope parameter	$G_1 = 0.61 \pm 0.02$	Huang et al. (2021)
Slope parameter	$G_2 = -0.006 \pm 0.006$	Huang et al. (2021)
Effective diameter	1.32 ± 0.06 km	Ishiguro et al. (2022)
Absolute mag (<i>V</i> filter)	17.54 ± 0.02	Ishiguro et al. (2022)
Sidereal period	5.234246 ± 0.000097 hr	This work (Section 3.1)
Bond albedo	0.052	Devogèle et al. (2020)
Geometric albedo	0.10 ± 0.02	Devogèle et al. (2020)
Color (<i>g</i> – <i>r</i>)	0.472 ± 0.05	This work (Section 4.1)
Color (<i>r</i> – <i>i</i>)	0.065 ± 0.05	This work (Section 4.1)
Shape aspect ratio	1.45	This work (Section 3.2)
Spin axis (preferred)	$\lambda_p = 116^\circ 6, \beta_p = -53^\circ 6$	This work (Section 3.2)
Spin axis	$\lambda = 300^\circ 3, \beta = -55^\circ 4$	This work (Section 3.2)
Mass-loss rate	0.04–0.37 kg s ⁻¹	This work (Section 4.3)
Critical density	570 kg m ⁻³	Jewitt & Hsieh (2006)
Photometric range	0.4	Jewitt & Hsieh (2006)
Thermophysics		
Thermal inertia	300 ⁺¹²⁰ ₋₁₁₀ J m ⁻² K ⁻¹ s ^{-1/2}	Devogèle et al. (2020)
Grain size	0.9–10 mm	Devogèle et al. (2020)
Mass-loss rate	≲0.1 kg m ⁻¹	Kasuga & Masiero (2022)

Table A1
(Continued)

Parameter	Value	Reference
Polarimetry ^a		
Max degree of neg. polarization	$P_{\min} = -1.2\% \pm 0.1\%$	Devogèle et al. (2020)
Phase where P_{\min} occurs	$\alpha_{\min} = 9^{\circ}5 \pm 0^{\circ}2$	Devogèle et al. (2020)
Inversion angle	$\alpha_{\text{inv}} = 20^{\circ}2 \pm 0^{\circ}2$	Devogèle et al. (2020)
Slope at α_{inv}	$h = 0.22\% \pm 0.01\%$	Devogèle et al. (2020)
Geometric albedo	$p_{\text{R}} = 0.1$	Ishiguro et al. (2022)

Note.

^a Additional polarimetric results are contained in Ishiguro et al. (2022) that are too broad for this table.

Appendix B 2005 UD Observations

Tables B1, B2, and B3 describe all observations used in this work including those rejected from the shape modeling procedure.

Table B1
Observational Circumstances

#	Date/Time End (deg)	Span	Telescope (UT)	Filter (hr)	N_p	m_V	r	Δ	\angle_{STO} (au)	Reference (au)
1	2005-Nov-2 11:54:32	3.26	LOT	R	6	18.3	1.37	0.55	36.7	1
2	2005-Nov-3 12:11:24	3.22	LOT	R	5	18.4	1.39	0.57	36.7	1
3	2005-Nov-4 12:05:20	3.00	LOT	R	13	18.5	1.4	0.59	36.7	1
4	2005-Nov-5 11:52:45	1.78	LOT	R	16	18.6	1.41	0.61	36.6	1
5	2005-Nov-19 08:50:19	0.56	UH88	R	15	19.6	1.57	0.91	35.9	2
6	2005-Nov-20 07:23:39	0.79	UH88	R	16	19.7	1.58	0.93	35.9	2
7	2005-Nov-21 05:48:28	3.19	UH88	R	17	19.8	1.59	0.95	35.8	2
8	2005-Nov-22 05:31:34	3.53	UH88	R	9	19.9	1.61	0.99	35.7	2
9	2018-Sep-27 00:49:29	1.97	LCO-fl16	r	92	16.6	1.09	0.23	62.5	4
10 ^a	2018-Sep-27 07:09:27	5.23	31in	...	87	16.5	1.1	0.22	58.2	4
11	2018-Sep-27 16:35:01	1.97	LCO-fl11	r	114	16.5	1.1	0.22	58.2	4
12	2018-Oct-1 15:55:45	2.47	LCO-fl11	r	115	16.1	1.16	0.23	40.6	4
13	2018-Oct-1 23:39:44	2.45	LCO-fl16	r	122	16.1	1.16	0.23	40.6	4
14	2018-Oct-3 05:41:52	2.45	LCO-fa15	r	142	16	1.18	0.23	36.3	4
15	2018-Oct-3 21:57:50	0.29	Ondřejov	R	17	15.9	1.2	0.24	28.0	5
16	2018-Oct-3 23:22:49	1.46	Ondřejov	R	134	15.9	1.2	0.24	28.0	5
17	2018-Oct-3 23:50:50	2.98	LCO-fl16	r	146	15.9	1.2	0.24	28.0	4
18	2018-Oct-4 00:51:58	0.96	Ondřejov	R	86	15.9	1.2	0.24	28.0	5
19	2018-Oct-4 02:20:05	1.63	Ondřejov	R	110	15.9	1.2	0.24	28.0	5
20	2018-Oct-5 21:17:57	2.18	Ondřejov	R	158	15.9	1.22	0.24	24.1	5
21	2018-Oct-5 23:32:08	1.97	Ondřejov	R	140	15.9	1.22	0.24	24.1	5
22	2018-Oct-5 01:31:54	2.23	Ondřejov	R	160	15.9	1.22	0.24	24.1	5
23 ^a	2018-Oct-6 04:07:48	8.38	31in	r	32	15.9	1.23	0.25	20.4	4
24	2018-Oct-6 02:59:19	6.29	TRAPPIST-S	R	348	15.9	1.23	0.25	20.4	4
25	2018-Oct-9 20:40:28	1.30	Ondřejov	R	80	15.8	1.27	0.28	10.6	5
26	2018-Oct-9 22:00:18	2.26	Ondřejov	R	154	15.8	1.27	0.28	10.6	5
27	2018-Oct-9 00:17:27	1.92	Ondřejov	R	125	15.8	1.27	0.28	10.6	5
28	2018-Oct-9 02:17:16	0.46	Ondřejov	R	28	15.8	1.27	0.28	10.6	5
29	2018-Oct-9 13:45:09	3.46	LCO-fl11	r	155	15.8	1.27	0.28	10.6	4
30	2018-Oct-9 20:30:22	3.55	LCO-fl06	r	168	15.8	1.27	0.28	10.6	4

Note. Date/Time: start of observations; Span: duration of observations; N_p : number of points; m_V : 2005 UD apparent V-band magnitude; r : Sun–target distance; Δ : Earth–target distance; \angle_{STO} : Sun–target–observer (phase) angle; LOT: Lulin One-meter Telescope; UH88: University of Hawaii 88-inch Telescope; LCO: Las Cumbres Observatory; 31in: Lowell Observatory NURO 31-inch Telescope; Ondřejov: Ondřejov Observatory 0.65 m Telescope; TRAPPIST-S: South TRAnsiting Planets and Planetesimals Small Telescope.

References. (1) Kinoshita et al. 2007; (2) Jewitt & Hsieh 2006; (3) Warner & Stephens 2019; (4) Devogèle et al. 2020; (5) this work.

^a Rejected from the inversion process due to excessive photometric noise or temporal overlap with other data.

Table B2
Observational Circumstances

#	Date/Time End (deg)	Span	Telescope (UT)	Filter (hr)	N_p	m_V	r	Δ	\angle_{STO} (au)	Reference (au)
31	2018-Oct-10 00:04:14	5.45	TRAPPIST-N	<i>R</i>	285	15.8	1.29	0.29	7.7	4
32	2018-Oct-10 00:30:22	2.69	Ondřejov	<i>R</i>	154	15.8	1.29	0.29	7.7	5
33 ^a	2018-Oct-10 03:09:27	9.02	31in	...	57	15.8	1.29	0.29	7.7	4
34	2018-Oct-10 04:59:36	2.28	LCO-fa15	<i>r</i>	112	15.8	1.29	0.29	7.7	4
35	2018-Oct-12 20:38:08	3.17	Ondřejov	<i>R</i>	107	15.8	1.31	0.31	2.6	5
36	2018-Oct-12 23:49:46	2.09	Ondřejov	<i>R</i>	114	15.8	1.31	0.31	2.6	5
37	2018-Oct-12 06:00:36	1.34	CS3	<i>V</i>	26	15.8	1.31	0.31	2.6	3
38	2018-Oct-12 08:15:57	2.54	CS3	<i>V</i>	26	15.8	1.31	0.31	2.6	3
39	2018-Oct-13 05:10:00	1.90	LCO-fa15	<i>r</i>	88	15.7	1.33	0.33	0.6	4
40	2018-Oct-13 12:04:43	3.36	LCO-fl11	<i>r</i>	153	15.7	1.33	0.33	0.6	4
41	2018-Oct-14 19:55:12	0.46	Ondřejov	<i>R</i>	19	15.9	1.34	0.34	2.1	5
42	2018-Oct-14 12:13:49	2.50	LCO-fl11	<i>r</i>	122	15.9	1.34	0.34	2.1	4
43	2018-Oct-15 18:47:03	2.69	Ondřejov	<i>R</i>	120	16.2	1.35	0.35	4.1	5
44	2018-Oct-15 21:29:53	2.54	Ondřejov	<i>R</i>	121	16.2	1.35	0.35	4.1	5
45 ^a	2018-Oct-15 02:26:25	9.10	31in	<i>r</i>	48	16.2	1.35	0.35	4.1	4
46	2018-Oct-15 03:32:17	1.49	CS3	<i>V</i>	27	16.2	1.35	0.35	4.1	3
47	2018-Oct-15 05:07:32	1.68	CS3	<i>V</i>	37	16.2	1.35	0.35	4.1	3
48	2018-Oct-15 06:56:53	1.80	CS3	<i>V</i>	31	16.2	1.35	0.35	4.1	3
49	2018-Oct-15 09:02:17	1.90	CS3	<i>V</i>	37	16.2	1.35	0.35	4.1	3
50	2018-Oct-15 19:22:50	1.75	LCO-fl16	<i>r</i>	60	16.2	1.35	0.35	4.1	4
51	2018-Oct-16 01:59:55	3.98	LCO-fa15	<i>r</i>	171	16.4	1.36	0.37	5.9	4
52 ^a	2018-Oct-16 02:24:27	3.17	31in	<i>r</i>	14	16.4	1.36	0.37	5.9	4
53	2018-Oct-16 03:13:13	1.75	CS3	<i>V</i>	22	16.4	1.36	0.37	5.9	3
54	2018-Oct-16 05:00:16	1.54	CS3	<i>V</i>	27	16.4	1.36	0.37	5.9	3
55	2018-Oct-16 06:42:44	3.26	CS3	<i>V</i>	52	16.4	1.36	0.37	5.9	3
56	2018-Oct-16 09:59:22	0.74	CS3	<i>V</i>	15	16.4	1.36	0.37	5.9	3
57	2018-Oct-16 12:15:49	0.36	LCO-fl12	<i>r</i>	14	16.4	1.36	0.37	5.9	4
58	2018-Oct-16 19:59:50	3.48	LCO-fl16	<i>r</i>	132	16.4	1.36	0.37	5.9	4
59	2018-Oct-16 21:42:10	2.71	Ondřejov	<i>R</i>	23	16.6	1.38	0.38	7.6	5
60	2018-Oct-17 02:59:36	3.46	LCO-fa15	<i>r</i>	150	16.6	1.38	0.38	7.6	4

Notes. Date/Time: start of observations; Span: duration of observations; N_p : number of points; m_V : 2005 UD apparent *V*-band magnitude; r : Sun–target distance; Δ : Earth–target distance; \angle_{STO} : Sun–target–observer (phase) angle; TRAPPIST-N: North TRAnsiting Planets and Planetesimals Small Telescope; Ondřejov: Ondřejov Observatory 0.65 m Telescope; Lowell Observatory NURO 31-inch Telescope; LCO: Las Cumbres Observatory; CS3: Center for Solar System Studies.

References. (1) Kinoshita et al. 2007; (2) Jewitt & Hsieh 2006; (3) Warner & Stephens 2019; (4) Devogèle et al. 2020; (5) this work.

^a Rejected from the inversion process due to excessive photometric noise or temporal overlap with other data.

Table B3
Observational Circumstances

#	Date/Time End (deg)	Span	Telescope (UT)	Filter (hr)	N_p	m_V	r	Δ	\angle_{STO} (au)	Reference (au)
61	2018-Oct-17 04:20:39	3.12	TRAPPIST-N	<i>R</i>	179	16.6	1.38	0.38	7.6	4
62	2018-Oct-17 18:52:22	2.30	Ondřejov	<i>R</i>	76	16.7	1.39	0.4	9.3	5
63	2018-Oct-17 21:11:36	2.69	Ondřejov	<i>R</i>	91	16.7	1.39	0.4	9.3	5
64	2018-Oct-20 23:58:39	2.28	TRAPPIST-N	<i>r</i>	133	17	1.41	0.43	12.1	4
65	2018-Oct-20 01:41:08	2.30	LCO-fa15	<i>r</i>	91	17	1.41	0.43	12.1	4
66	2018-Oct-25 10:28:53	3.77	LCO-fl12	<i>r</i>	75	17.7	1.47	0.51	17.8	4
67	2018-Oct-27 01:43:35	2.98	LCO-fa15	<i>r</i>	69	17.9	1.5	0.55	19.6	4
68	2018-Oct-28 00:08:31	3.43	LCO-fa03	<i>r</i>	84	18.1	1.5	0.56	20.4	4
69	2018-Oct-30 10:38:14	3.46	LCO-fl11	<i>r</i>	73	18.3	1.53	0.6	21.9	4
70	2018-Oct-31 10:24:58	3.02	LCO-fl11	<i>r</i>	60	18.4	1.54	0.62	22.6	4
71	2018-Nov-1 01:42:22	2.93	LCO-fa15	<i>r</i>	62	18.5	1.55	0.64	23.2	4
72	2018-Nov-2 02:43:58	1.90	LCO-fa15	<i>r</i>	43	18.6	1.56	0.67	23.8	4
73	2018-Nov-4 00:24:18	4.06	Danish	<i>R</i>	20	18.8	1.58	0.69	24.8	5
74 ^b	2019-Oct-18 09:19:18	3.24	LDT	<i>VR</i>	83	20.3	1.66	1.16	36.3	5
75	2019-Nov-3 01:20:13	5.16	NOT	<i>r</i>	329	19.6	1.49	0.87	39.6	5
76	2019-Nov-18 07:24:19	5.81	LDT	<i>VR</i>	666	18.8	1.32	0.66	45.2	5
77	2019-Nov-18 01:15:07	5.47	NOT	<i>gri</i>	254	18.8	1.33	0.66	45.8	5
78	2019-Nov-23 00:25:28	5.52	TRAPPIST-N	<i>Rc</i>	130	18.6	1.25	0.58	50.7	5
79	2019-Nov-24 02:10:49	2.57	TRAPPIST-N	<i>Rc</i>	62	18.5	1.23	0.56	51.7	5
80 ^a	2019-Nov-25 00:34:05	5.57	TRAPPIST-N	<i>Rc</i>	115	18.5	1.22	0.55	52.7	5
81	2021-Oct-27 03:30:14	0.65	Danish	<i>R</i>	8	19.2	1.90	0.92	7.2	5
82	2021-Oct-28 03:11:31	1.27	Danish	<i>R</i>	13	19.3	1.91	0.93	7.7	5
83	2021-Oct-29 00:05:46	3.58	Danish	<i>R</i>	19	19.3	1.91	0.94	8.2	5
84	2021-Oct-30 00:02:53	3.56	Danish	<i>R</i>	25	19.4	1.92	0.95	8.7	5
85	2021-Nov-301:29:31	2.47	LDT	<i>VR</i>	115	19.6	1.95	1.00	11.2	5
86	2005–2011 SPARSE	...	CSS	<i>V</i>	19	6
87	2014–2021 SPARSE	...	PS	<i>w</i>	31	7
88	2018–2021 SPARSE	...	ZTF	<i>V</i>	71	8
89	2005–2011 SPARSE	...	ATLAS	<i>o</i>	41	9
90	2005–2011 SPARSE	...	CSS	<i>G</i>	44	6

Notes. Date/Time: start of observations; Span: duration of observations; N_p : number of points; m_V : 2005 UD apparent *V*-band magnitude; r : Sun–target distance; Δ : Earth–target distance; \angle_{STO} : Sun–target–observer (phase) angle; TRAPPIST-N: North TRAnsiting Planets and Planetesimals Small Telescope; Ondřejov: Ondřejov Observatory 0.65 m Telescope; LCO: Las Cumbres Observatory; LDT: Lowell Discovery Telescope; NOT: Nordic Optical Telescope; Danish: La Silla Observatory 1.54 m Telescope; CSS: Catalina Sky Survey; PS: Pan-STARRS; ZTF: Zwicky Transient Facility; ATLAS: Asteroid Terrestrial-impact Last Alert System.

References. (1) Kinoshita et al. 2007; (2) Jewitt & Hsieh 2006; (3) Warner & Stephens 2019; (4) Devogèle et al. 2020; (5) this work; (6) Larson et al. 2003; (7) Chambers et al. 2016; (8) Bellm et al. 2019; (9) Tonry et al. 2018.

^a Rejected from the inversion process due to excessive photometric noise or temporal overlap with other data.


^b First 1.5 hr rejected from the inversion process due to being inconsistent with our best-fit models.

ORCID iDs


Jay K. Kueny  <https://orcid.org/0000-0001-8531-038X>

Colin Orion Chandler  <https://orcid.org/0000-0001-7335-1715>

Maxime Devogèle  <https://orcid.org/0000-0002-6509-6360>


Nicholas Moskovitz  <https://orcid.org/0000-0001-6765-6336>

Petr Pravec  <https://orcid.org/0000-0001-8434-9776>

Hana Kučáková  <https://orcid.org/0000-0002-1330-1318>

Kamil Hornoch  <https://orcid.org/0000-0002-0835-225X>

Peter Kušnirák  <https://orcid.org/0000-0001-6098-6893>

Mikael Granvik  <https://orcid.org/0000-0002-5624-1888>

Christina Konstantopoulou  <https://orcid.org/0000-0002-4690-0157>


Nicholas E. Jannsen  <https://orcid.org/0000-0003-4670-9616>

Shane Moran  <https://orcid.org/0000-0001-5221-0243>

Lauri Siltala  <https://orcid.org/0000-0002-6938-794X>

Grigori Fedorets  <https://orcid.org/0000-0002-8418-4809>

Marin Ferrais  <https://orcid.org/0000-0002-0535-652X>

Emmanuel Jehin  <https://orcid.org/0000-0001-8923-488X>

Theodore Kareta  <https://orcid.org/0000-0003-1008-7499>

Josef Hnuš  <https://orcid.org/0000-0002-2934-3723>

References

- Ahn, C. P., Alexandroff, R., Allende Prieto, C., et al. 2012, *ApJS*, 203, 21
- Astropy Collaboration, Robitaille, T. P., Tollerud, E. J., et al. 2013, *A&A*, 558, A33
- Bellm, E. C., Kulkarni, S. R., Graham, M. J., et al. 2019, *PASP*, 131, 018002
- Bertin, E. 2006, in ASP Conf. Ser. 351, *Astronomical Data Analysis Software and Systems XV*, ed. C. Gabriel et al. (San Francisco, CA: ASP), 112
- Bertin, E., & Arnouts, S. 1996, *A&AS*, 117, 393
- Bottke, W. F., Vokrouhlický, D., Rubincam, D. P., & Nesvorný, D. 2006, *AREPS*, 34, 157
- Breiter, S., Nesvorný, D., & Vokrouhlický, D. 2005, *AJ*, 130, 1267
- Busch, M. W., Ostro, S. J., Benner, L. A. M., et al. 2011, *Icar*, 212, 649
- Cellino, A., Bagnulo, S., Gil-Hutton, R., et al. 2015, *MNRAS*, 451, 3473
- Chambers, K. C., Magnier, E. A., Metcalfe, N., et al. 2016, arXiv:1612.05560
- Chandler, C. O., Kueny, J. K., Trujillo, C. A., Trilling, D. E., & Oldroyd, W. J. 2020, *ApJL*, 892, L38

- Chandler, C. O., Trujillo, C. A., & Hsieh, H. H. 2021, *ApJL*, **922**, L8
- Christensen, E., Beshore, E., Garradd, G., et al. 2005, 2005 UD, Tech. Rep. MPEC 2005-U22 (Cambridge, MA: Minor Planet Center), <https://minorplanetcenter.net//mpec/K05/K05U22.html>
- Devogèle, M., MacLennan, E., Gustafsson, A., et al. 2020, *PSJ*, **1**, 15
- Dobrovolskis, A. R. 1996, *Icar*, **124**, 698
- Dundon, L. 2005, Master's thesis, Univ. Hawai'i at Manoa
- Đurech, J., Vokrouhlický, D., Kaasalainen, M., et al. 2008, *A&A*, **488**, 345
- Flewelling, H. A., Magnier, E. A., Chambers, K. C., et al. 2020, *ApJS*, **251**, 7
- Gaia Collaboration, Brown, A. G. A., Vallenari, A., et al. 2018, *A&A*, **616**, A1
- Giorgini, J. D., Yeomans, D. K., Chamberlin, A. B., et al. 1996, AAS/DPS Meeting, **28**, 25.04
- Hanuš, J., Delbo', M., Vokrouhlický, D., et al. 2016, *A&A*, **592**, A34
- Hanuš, J., Durech, J., Brož, M., et al. 2011, *A&A*, **530**, A134
- Hanuš, J., Vokrouhlický, D., Delbo, M., et al. 2018, *A&A*, **620**, L8
- Huang, J. N., Muinonen, K., Chen, T., & Wang, X. B. 2021, *P&SS*, **195**, 105120
- Ishiguro, M., Bach, Y. P., Geem, J., et al. 2022, *MNRAS*, **509**, 4128
- Jacobson, S. A., & Scheeres, D. J. 2011, *Icar*, **214**, 161
- Jehin, E., Gillon, M., Queloz, D., et al. 2011, *Msngr*, **145**, 2
- Jewitt, D. 2012, *AJ*, **143**, 66
- Jewitt, D. 2013, *AJ*, **145**, 133
- Jewitt, D. 2021, *AJ*, **161**, 261
- Jewitt, D., & Hsieh, H. 2006, *AJ*, **132**, 1624
- Jewitt, D., & Li, J. 2010, *AJ*, **140**, 1519
- Jordi, K., Grebel, E. K., & Ammon, K. 2006, *A&A*, **460**, 339
- Joye, W. A., & Mandel, E. 2003, in ASP Conf. Ser. 295, *Astronomical Data Analysis Software and Systems XII*, ed. H. E. Payne, R. I. Jedrzejewski, & R. N. Hook (San Francisco, CA: ASP), 489
- Kaasalainen, M., Durech, J., Warner, B. D., Krugly, Y. N., & Gaftonyuk, N. M. 2007, *Natur*, **446**, 420
- Kaasalainen, M., & Torppa, J. 2001, *Icar*, **153**, 24
- Kaasalainen, M., Torppa, J., & Muinonen, K. 2001, *Icar*, **153**, 37
- Kareta, T., Reddy, V., Pearson, N., Sanchez, J. A., & Harris, W. M. 2021, *PSJ*, **2**, 190
- Kasuga, T., & Jewitt, D. 2008, *AJ*, **136**, 881
- Kasuga, T., & Masiero, J. R. 2022, *AJ*, **164**, 193
- Kim, M.-J., Lee, H.-J., Lee, S.-M., et al. 2018, *A&A*, **619**, A123
- Kinoshita, D., Ohtsuka, K., Sekiguchi, T., et al. 2007, *A&A*, **466**, 1153
- Kipreos, Y., Campbell-Brown, M., Brown, P., & Vida, D. 2022, *MNRAS*, **516**, 924
- Laher, R. R., Gorjian, V., Rebull, L. M., et al. 2012, *PASP*, **124**, 737
- Landolt, A. U. 1992, *AJ*, **104**, 340
- Larson, S., Beshore, E., Hill, R., et al. 2003, AAS/DPS Meeting, **35**, 36.04
- Lee, H.-J., Kim, M.-J., Kim, D.-H., et al. 2019, *P&SS*, **165**, 296
- Li, J., & Jewitt, D. 2013, *AJ*, **145**, 154
- Licandro, J., Campins, H., Mothé-Diniz, T., Pinilla-Alonso, N., & de León, J. 2007, *A&A*, **461**, 751
- MacLennan, E., Marshall, S., & Granvik, M. 2022, *Icar*, **388**, 115226
- MacLennan, E., Toliou, A., & Granvik, M. 2021, *Icar*, **366**, 114535
- Mainzer, A., Bauer, J., Cutri, R. M., et al. 2014, *ApJ*, **792**, 30
- Masiero, J., Wright, E., & Mainzer, A. 2019, *AJ*, **158**, 97
- Mommert, M. 2017, *A&C*, **18**, 47
- Moskovitz, N., Wasserman, L., Burt, B., et al. 2022, *A&C*, **41**, 100661
- Naidu, S. P., Margot, J. L., Taylor, P. A., et al. 2015, *AJ*, **150**, 54
- Ochsenbein, F., Bauer, P., & Marcout, J. 2000, *A&AS*, **143**, 23
- Ohtsuka, K., Arakida, H., Ito, T., Yoshikawa, M., & Asher, D. J. 2008, *M&PSA*, **43**, 5055
- Ohtsuka, K., Sekiguchi, T., Kinoshita, D., et al. 2006, *A&A*, **450**, L25
- Ostro, S. J., Margot, J.-L., Benner, L. A. M., et al. 2006, *Sci*, **314**, 1276
- Pravec, P., Fatka, P., Vokrouhlický, D., et al. 2019, *Icar*, **333**, 429
- Pravec, P., Scheirich, P., Durech, J., et al. 2014, *Icar*, **233**, 48
- Pravec, P., Vokrouhlický, D., Polishook, D., et al. 2010, *Natur*, **466**, 1085
- Rozek, A., Lowry, S. C., Rozitis, B., et al. 2019, *A&A*, **627**, A172
- Rubincam, D. P. 2000, *Icar*, **148**, 2
- Ryabova, G., Avdyushev, V., & Williams, I. 2019, *MNRAS*, **485**, 3378
- Ryabova, G. O. 2017, *P&SS*, **143**, 125
- SciPy 1.0 Contributors, Virtanen, P., Gommers, R., et al. 2020, *NatMe*, **17**, 261
- Skiff, B. A., Buie, M. W., & Bowell, E. 1996, AAS/DPS Meeting, **28**, 10.36
- Sonka, A. B., Birlan, M., Anghel, S., et al. 2019, *RoAJ*, **29**, 33
- Steckloff, J. K., & Jacobson, S. A. 2016, *Icar*, **264**, 160
- Tardioli, C., Farnocchia, D., Rozitis, B., et al. 2017, *A&A*, **608**, A61
- Tonry, J. L., Denneau, L., Heinze, A. N., et al. 2018, *PASP*, **130**, 064505
- Warner, B. D., & Stephens, R. D. 2019, *MPBu*, **46**, 144
- Whipple, F. L. 1983, *IAUC*, **3881**, 1
- Ye, Q., Knight, M. M., Kelley, M. S. P., et al. 2021, *PSJ*, **2**, 23